WSRC-MS-2002-00693 Rev. 1

Mechanistic Modeling of Porosity In Hanford 3013 Outer Container Welds (U)

By

W. L. Daugherty
G. R. Cannell

Submitted for publication in Science and Technology of Welding and Joining

1.0 INTRODUCTION

One of the current priorities within the Department of Energy (DOE) complex is the stabilization, packaging and storage of plutonium-bearing materials. The packaging is key to the safe long-term handling and storage of these materials. Packaging consists of placing the stabilized materials into a set of two nested stainless steel containers. Each container is seal-welded, providing double containment of the plutonium materials (see Figure 1). The outer container is designated as the primary barrier to the release of the materials to the environment.

The outer container assembly is fabricated from Type 316L stainless steel. The lid is inserted into the outer container to create an interference fit that forms a square-groove, corner joint that is subsequently sealed by depositing a full-penetration, autogenous, GTAW weld - See Figure 2. The GTAW closure-welding system was developed and qualified at the Savannah River Site (SRS) and shipped to the Plutonium Finishing Plant (PFP), at the DOE Hanford Site, where it is used to package plutonium-bearing materials. The closure welding system and qualification efforts are described in References 1 and 2.

The outer container and closure weld comply with the design, fabrication and examination rules of the ASME Section VIII code, to the extent feasible. Post closure-weld hydrostatic testing is not practicable due to the presence of the packaged waste. In an effort to establish an equivalent level of weld quality, sensitive leak testing of each production closure and periodic (1 in 25 production closures) radiographic and metallographic examination of test containers (production outer containers with non-radioactive surrogate materials) are specified. During production operations, volumetric examination of these periodic test welds identified a trend in which porosity (typically a single pore of spherical shape) may form at the weld tie-in (the point at which the weld puddle intercepts the weld start). A limited number of these pores failed to meet specified acceptance criteria by exceeding the maximum allowable diameter.

An initial, full scope diagnostic analysis of the equipment, welding materials / consumables and process conditions identified the primary cause of the porosity to be related to geometry at the root of the weld joint preparation. A volume of gas is trapped between the advancing weld puddle and the start of the weld, at weld tie-in, and incorporated into the weld during puddle solidification. Figure 5 illustrates the basic geometric conditions contributing to the porosity. This paper describes the efforts to analyze and understand / quantify the interaction between the weld-joint geometry and formation of porosity at the weld tie-in. It is noted that the data suggest other contributing factors that were not studied in detail as part of this work. The driver for this effort was to resolve the porosity trend to the extent necessary to produce production-quality welds. A simple re-design of the weld-joint geometry, identified as the primary contributor to the porosity trend, was performed, resolving the production weld quality concerns.

Geometric Elements at the Root of the Closure Weld Joint

The lids are machined with a continuous radius of less than 0.005 inch at the inside corner where the lid plug and flange surfaces meet. The outer container receives a 45 degree chamfer on the top ID edge – See Figure 3. The chamfer (leg dimension) was measured on a number of containers and found to vary from approximately 0.005 inch to 0.016 inch.

Additionally, lid bottom and container top surfaces were measured to characterize flatness at the point where these two surfaces meet to form the square-groove weld joint when assembled. Container top surfaces were typically very flat with runout of less than 0.001 inch. The bottom surface of the lid flanges, however, was inconsistent with measured runout of up to 0.006 inch, though most were typically 0.003 inch. Theoretically, if the container top surface and lid flange had no runout, a fully inserted lid would produce no "axial gap" or separation of the square-groove. However, due to the actual lid flange runout, contact between the flange and the container top is not continuous, creating local axial gaps at the groove side-wall surfaces.

Test and Analysis

Testing and data collection were performed in two steps. The first step involved making and characterizing weld segments from which a detailed geometric description of weld bead shape and weld-joint preparation at the weld tie-in was developed. With this geometric description, the volume of gas trapped at the tie-in was calculated and a working model describing pore formation and size developed. The second step involved making and examining a number of welds with varying chamfer and axial gap to refine and validate the porosity model.

Data

A container/lid assembly was welded such that the normal tack weld sequence was followed by deposition of four weld segments. Each segment was approximately 2 to 3 inches long employing the normal weld start sequence, but terminated abruptly without the normal welding downslope. The axial gap between the container and lid was characterized prior to welding, and again immediately after the tack welds were made but prior to making the weld segments. Initial gaps ranged from 0.000 to 0.004 inch. After tacking, the maximum gap size measured was 0.002 inch. Weld segments were located to start and stop in regions with different axial gaps.

Following welding of the four segments, the container was cross-sectioned to measure the final axial gap and characterize the weld bead shape at the start and stop locations for each segment. Figure 4 shows a section of the container/lid joint preparation about 1/8 inch away from the start of a weld segment. The start and stop locations of all four segments were similar and showed no significant axial gap, regardless of the magnitude of the pre-weld gap. The area created between the chamfer face and lid radius can be seen in this figure. Two of the start positions and two of the stop positions were further sectioned through the weld center to characterize weld bead shape along the weld axis - See Figure 5. In this figure it can be seen that at the moment the face of the advancing

weld bead intercepts the start of the weld, there exists a length of unwelded or unfused chamfer (black area). A volume associated with the chamfer can now be calculated by multiplying the unfused chamfer length by the chamfer area seen in the Figure 4 cross-section. Likewise, it is noted that there exists a portion of unfused square-groove preparation for which, in the presence of an axial gap, an additional volume of gas can be calculated.

Following characterization of the weld bead geometry, 35 test welds were made with varying chamfer and axial gap – a portion of these welds were made at Hanford and the remainder at SRS on the prototype of the Hanford system. Table 1 provides the details and results for these welds. The outer containers were machined to create various chamfer sizes. Axial gaps were established and verified through the use of shims and feeler gages. Chamfer size ranged from 0.004 to 0.022 inch, and pre-weld axial gaps ranged from <0.001 to 0.012 inch.

All welds were volumetrically examined by radiography to locate and characterize any pores that might be present.

Analysis of Trapped Volume

On the basis of the weld-bead shape and weld-joint geometry characterization at the start / stop areas noted above, the actual trapped gas volume that might contribute to porosity was calculated. At the time when a vent path through the face or front of the weld joint is just sealed (point at which the advancing weld bead intercepts the start of the weld), the unfused portion of the chamfer has a length of approximately 0.091 inch. Similarly, the unfused area of the square groove portion of the weld joint is approximately 0.00404 sq. inch (Figure 6). Based on these measurements, the trapped volume is calculated by:

$V = 0.00404 \text{ sq. in.} * \text{axial gap} + 0.091 \text{ in.} * ½ * (\text{chamfer length})^2$

Both axial gap and chamfer length are in inches, and the volume is in cubic inches. The diameter of a sphere of equal volume can be calculated with the following equation:

$\text{Sphere Dia.} = 1.2407 * \sqrt[3]{V}$

Since the calculation of trapped gas volume does not predict whether that gas will be divided among multiple pores, the actual pore sizes measured (in the event of multiple pores) were combined into an equivalent single pore diameter.

Further Analysis of Axial Gap

The model developed thus far follows the general trend in the data, but does not provide good agreement to the full data set. For example, the predicted impact of varying gap size is not supported by the data - See Figure 7.

The test welds are represented by three, separate groups in which axial gaps fall within the following ranges: <0.001 inch; 0.002 – 0.003 inch; and 0.010 – 0.012 inch. Based on the model, these different gap ranges would be expected to produce different pore sizes for similar chamfers. If this had occurred, then plotting the pore size as a function of chamfer should produce a distinct set of data for each gap range, with these sets offset laterally from each other. However, as seen in Figure 7 all three sets of data follow the same trend, with no offset. Accordingly, these data indicate that axial gaps up to 0.010 inch do not significantly impact the size of a pore. Dimensional measurements of the can and lid before and after welding indicate that axial gaps of up to 0.020 inch will disappear during the weld due to shrinkage forces. The model incorporates this effect by ignoring the first 0.020 inch of any pre-weld axial gap (where it exists).

Analysis of Temperature Effects

The average gas temperature is assumed to equal the average metal temperature surrounding it whether that metal is solid or molten. As the gas volume is trapped at the tie-in, the gas temperature will be high, but not as high as when it becomes fully enveloped by the molten weld puddle. As the gas temperature increases, there will be a corresponding increase in gas volume, since the puddle will not sustain any significant pressure increase. To maintain geometric control of the weld bead, a copper chill block is clamped to the top of the lid during welding. This copper chill block has been instrumented to record its temperature during welds. At a distance of ~1/8 inch above the lid the maximum temperature was 160 C. The temperature gradient between the weld puddle (at the melting temperature of the steel, 1400 C) and this location in the chill block can be calculated.

It is assumed that the temperature gradient surrounding the weld puddle is the same in all directions over a short distance (short in comparison to the distance from the puddle to the copper chill block on top of the lid). The top of the chamfer space is 0.157 inch from the top of the lid. Over the chamfer space, the weld puddle is 0.090 inch from the top of the lid (average dimension measured on metallographic cross-sections). These conditions are illustrated in Figure 8.

The temperature gradient will be steeper in the stainless steel lid than in the copper block, in proportion to the thermal conductivity of each material. While there is typically a temperature drop at an interface between two materials, it is noted that contact between the lid and copper block is sufficiently intimate that the copper block retains an impression of machining marks on the lid after each weld. Therefore, the temperature drop at the interface will be ignored. Therefore, the temperature gradient from the weld puddle (0.090 inch from the lid surface) to a location 1/8 inch into the copper block can be calculated.

The thermal conductivity of copper is 17 times greater than that of 316L stainless steel. Accordingly, the temperature gradient within the lid will be 17 times steeper than the gradient within the copper. Knowing the total temperature drop of 1400 – 160 = 1240 C, one can show that the temperature gradient within the lid is 13,260 C/inch and the

temperature gradient within the chill block is 780 C/inch. The average gas temperature within the unconsumed chamfer matches the metal temperature ~0.045 inches ahead of the weld puddle (based on 0.091 inch unconsumed chamfer). Therefore, the midpoint of the unconsumed chamfer has a temperature of (13260 C/inch * 0.045 inch =)597 C below the melting point, or 803 C. As the gas temperature increases from 803 C to 1400 C, the gas volume will increase by a factor of 1.55, and the diameter of a sphere containing the gas will increase by a factor of 1.16.

In close agreement with this result, it is seen that increasing the predicted pore diameter for SRS-made welds by a factor of 1.1 to account for thermal expansion provides nominal agreement between the calculated volume of trapped gas and the measured pore sizes. This agreement is seen in Figure 9. A consistent bias however, is observed between pore sizes in Hanford welds and SRS welds from that predicted by the model. It is observed that increasing the correction factor in the model from 1.1 to 1.5 improves agreement with the Hanford weld data - see Figure 10. Additional factor(s) leading to this bias have not been conclusively proven, but limited data suggest this difference may relate to the solvents used in cleaning the containers prior to welding.

During welding at Hanford, it was identified that the alcohol used for cleaning differs from that used at SRS. Hanford used 100% ethanol denatured with benzene, while SRS used 95% ethanol. The denaturant consists of small amounts of various organic compounds not found in 95% ethanol. The plastic bottle and lint-free cloths used to apply the alcohol can contain compounds that are dissolved by the denaturant (more so than by the 95% ethanol). These dissolved materials may leave a residue on the container/lid surfaces leading to the potential for weld-joint surface contamination. Regardless of cause, it is observed empirically that with the correction factor increased to 1.5 for Hanford welds, the porosity model provides good agreement.

Conclusions

Porosity in the 3013 Outer Container closure weld has been shown to correlate primarily to the chamfer length on the ID edge of the container top, and to a lesser extent to any pre-weld axial gap between the container and lid. The measured pore provides good agreement with that calculated from the volume trapped within the container chamfer. Additional gas that might be contained within an axial gap between the container and lid does not contribute significantly to the trapped volume.

Acknowledgements

The authors wish to recognize and thank the many individuals who contributed to the successful completion of this work. Welding, equipment and instrumentation support was provided by S. Breshears, D. Maxwell, T. Sessions and T. Usry of the Savannah River Site. The support of R. Gregory and his team at the Hanford Plutonium Finishing Plant is gratefully acknowledged.

References

1. G. Cannell, W. Daugherty, L. Gaston, S. Howard, P. Korinko, D. Maxwell, G. McKinney, C. Sessions and S. West, "GTA Welding Research and Development for Plutonium Containment", published in proceedings from 6th International Conference on Trends in Welding Research, April 2002, ASM International.
2. G. R. Cannell, W. L. Daugherty and M. W. Stokes, "Welds Safeguard Plutonium-Bearing Containers", Welding Journal, Vol. 81, No. 7, July 2002.

Figure 1. 3013 Outer Container (left) and Inner Container

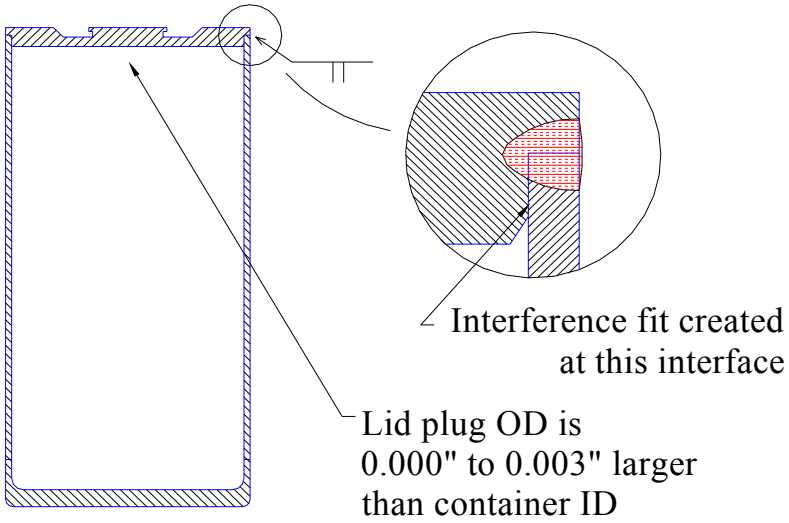

Figure 2. Interference Fit and Square-Groove Weld Joint Created when Lid is Inserted into the Outer Container

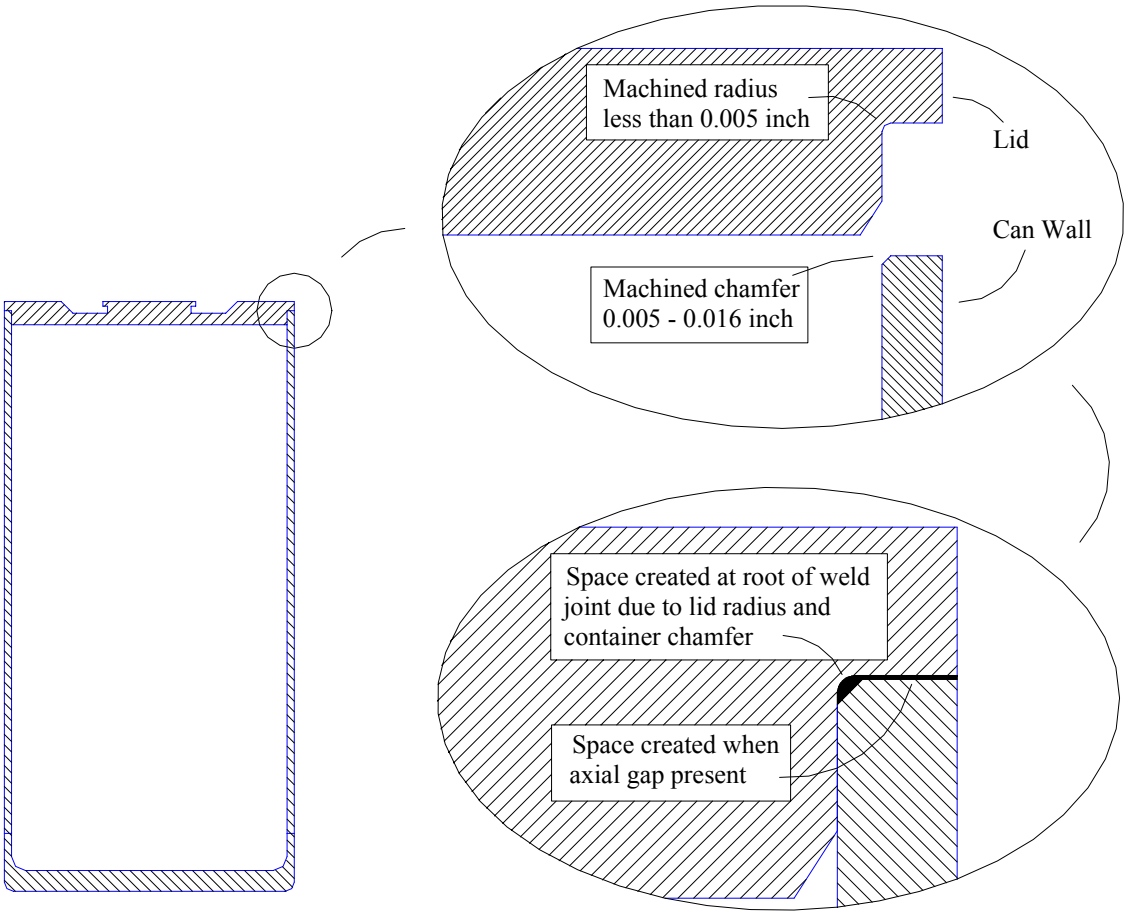

Figure 3. Lid Radius, Container Chamfer and Axial Gap Associated with the Weld Joint Preparation

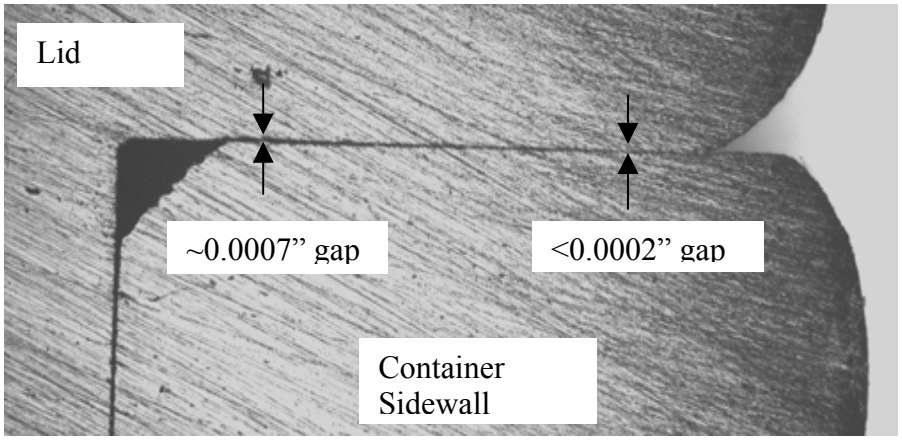

Figure 4.

Cross Section 1/8 inch from Start of Weld Segment with Initial Pre-Weld Axial Gap of 0.004 inch. Note the Extent to which the Axial Gap has Closed.

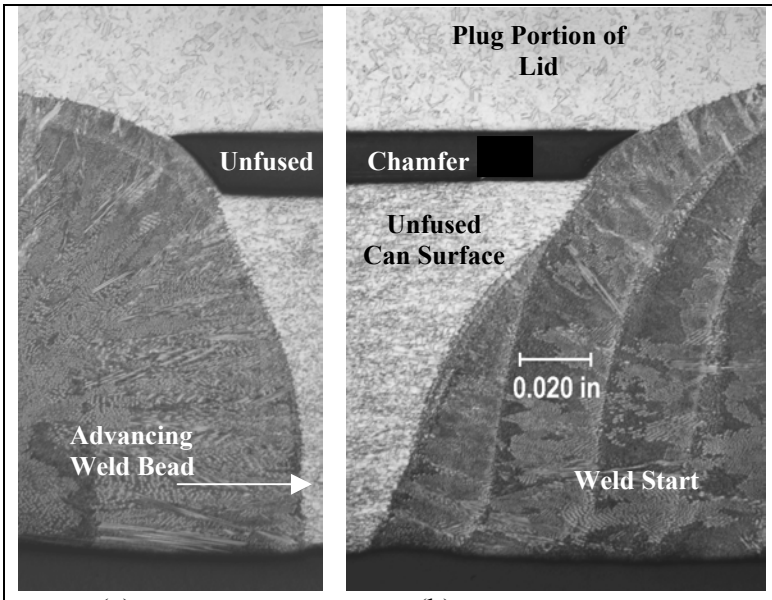

Figure 5.

Geometric Conditions which can Lead to Trapping a Gas Pocket at the Weld Tie-in.

(a) planar cross-section of weld just before tie-in
(b) planar cross-section of weld at start position

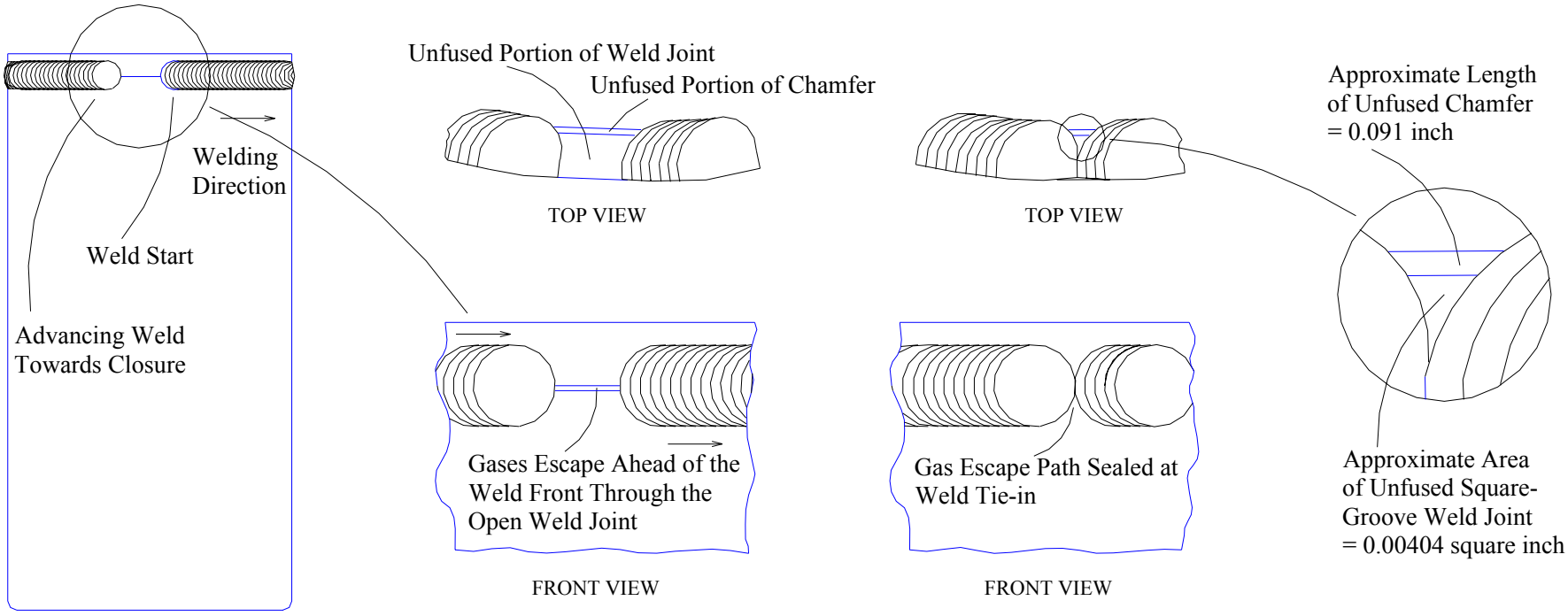

1. Weld Nearly Complete, Approaching Weld Tie-in
2. Gas Vents Through Open Weld Joint Face
3. Weld Tie-in
4. Geometry and Dimensions of Unfused Weld Joint at Tie-in

Figure 6. Geometry and Dimensions of Unfused Chamfer and Square-Groove Weld Preparation at Weld Tie-in

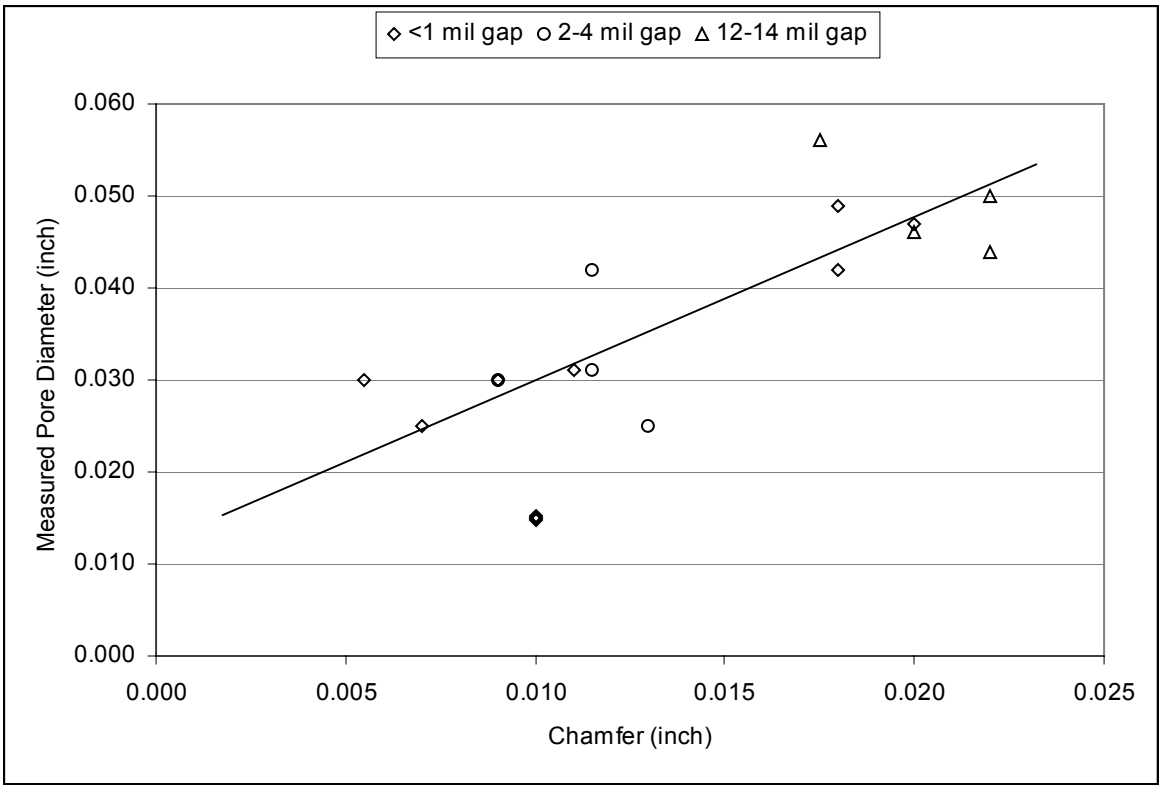

Figure 7. Relationship between pore diameter and container chamfer. Note that the data are clustered around the same trendline regardless of axial gap. The trend line is not specifically fit to the data, but is provided as a convenience to illustrate the consistency in the data set and the insensitivity of pore size to axial gap.

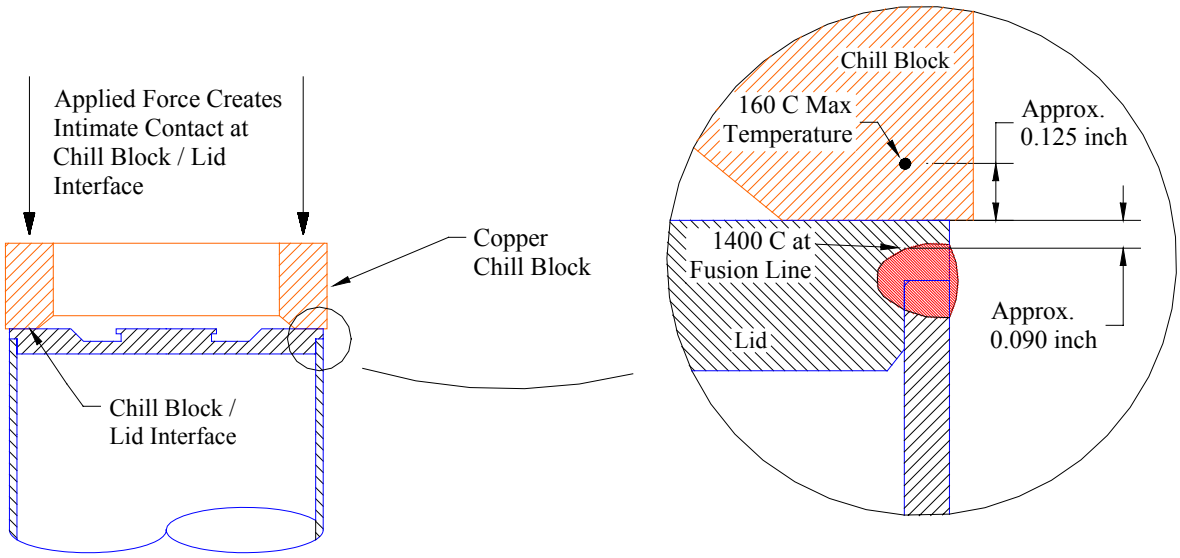

Figure 8. Temperature Data and Position Used to Analyze Temperature Effects

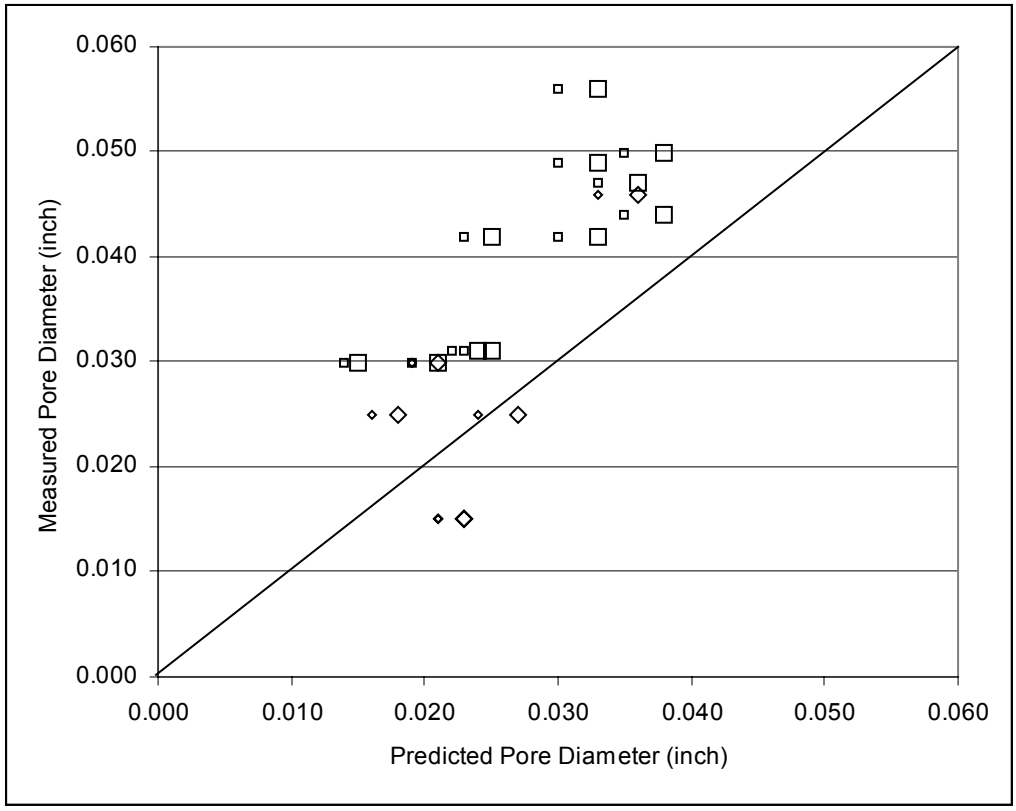

Figure 9. Comparison between predicted and actual pore size (squares are Hanford welds, diamonds are SRS welds) for welds containing porosity. The smaller symbols show the raw data, while the larger symbols incorporate a 1.1 temperature correction

factor. This factor gives good nominal agreement for the SRS welds, but not the Hanford welds.

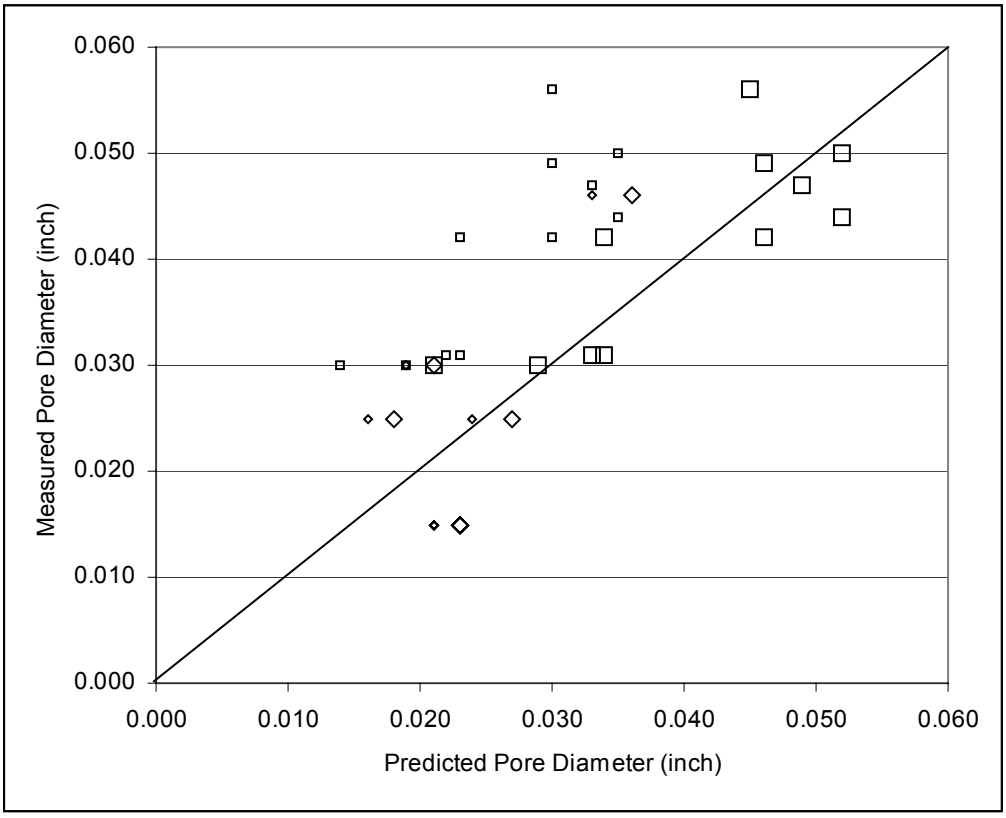

Figure 10. Comparison between predicted and actual pore size (squares are Hanford welds, diamonds are SRS welds). The smaller symbols show the raw data while the larger symbols incorporate a temperature correction factor of 1.1 for SRS welds and 1.5 for Hanford welds. These respective factors give good nominal agreement for both the SRS and Hanford welds. The predictive model is described in the text. For perfect agreement, the data points would lie on the line.

Table 1. Results of Test Welds

Weld Test ID	**Location of Weld**	**Axial Gap (inch)**	**Chamfer (inch)**	**No. of Pores**	**Pore Diameter (Inch)**
Gp-2	Hanford	<0.001	0.004	0	N/A
Gp-3	Hanford	<0.001	0.004	0	N/A
Gp-4	Hanford	<0.001	0.005	0	N/A
Gp-5	Hanford	<0.001	0.005	0	N/A
Gp-6	Hanford	<0.001	0.006	1	0.030
GP-7	Hanford	0.010	0.022	1	0.050
Gp-8	Hanford	0.011	0.018	1	0.056

Gp-9	Hanford	0.012	0.022	1	0.044
Gp-10	Hanford	<0.001	0.018	2	0.034, 0.043
Gp-11	Hanford	<0.001	0.018	2	0.020, 0.040
Gp-12	Hanford	<0.001	0.020	2	0.035, 0.040
Gp-13	Hanford	0.003	0.012	2	0.020, 0.040
Gp-14	Hanford	0.002	0.012	2	0.015, 0.030
Gp-15	Hanford	0.002	0.009	3	0.015, 0.020, 0.025
Gp-16	SRTC	<0.001	0.004	0	N/A
Gp-17	SRTC	<0.001	0.004	0	N/A
Gp-18	SRTC	<0.001	0.010	1	N/A
Gp-19	SRTC	<0.001	0.010	1	0.020
Gp-19x	SRTC	<0.001	0.010	1	0.015
Gp-20	SRTC	<0.001	0.009	0	N/A
Gp-21	SRTC	<0.001	0.009	3	0.015, 0.020, 0.025
Gp-22	SRTC	<0.001	0.008	0	N/A
Gp-23	SRTC	<0.001	0.008	0	N/A
Gp-24	SRTC	<0.001	0.007	1	0.025
Gp-25	SRTC	<0.001	0.007	0	N/A
Gp-26	SRTC	<0.001	0.006	0	N/A
Gp-27	SRTC	<0.001	0.006	0	N/A
Gp-28	SRTC	<0.001	N/A	0	N/A
Gp-29	SRTC	0.004	N/A	0	N/A
Gp-19a	SRTC	<0.001	0.011	2	0.015, 0.030
Gp-19b	SRTC	<0.001	0.011	0	N/A
Gp-19c	SRTC	<0.001	0.010	0	N/A
Gp-31	SRTC	0.000 – 0.004	0.014	0	N/A
Gp-32	SRTC	0.003	0.013	1	0.025
Gp-33	SRTC	0.011	0.020	2	0.020, 0.045